STATUS REPORT
OF THE EXPERIMENTAL AND THEORETICAL INVESTIGATIONS
IN THE GARCHING ELECTRON RING ACCELERATOR

C. Andelfinger, W. Dommaschk, J. Fink, W.Herrmann,
I. Hofmann, D. Jacobi, P. Merkel, H.-B. Schilling,
U. Schumacher, M. Ulrich *

Abstract

In the Pustarex electron ring accelerator low-intensity electron rings were accelerated without ions. Rings with larger electron numbers ran into instabilities with a radial precessional mode, which led to ring widening and particle losses. With resistive walls this instability - probably the resistive wall instability - occurred rather early. After replacement of the resistive walls by capacitive walls the instability happened mostly at the end of compression. Rearrangement of the system is planned to improve the symmetry of the fields and enhance the Landau damping coefficient. To increase the negative mass threshold of the number of trapped electrons in the ring, a beam with instantaneous energy spread has been developed. An arrangement which results in a beam with two energy peaks 5% apart is described. Also connected with the negative mass instability are calculations of the coupling impedance of an electron ring to a realistic squirrel cage. A few of the results, which show a rather large impedance with additional resonances, are presented.

The present paper reports three main subjects:
1. the experiments with the Garching Pustarex electron ring accelerator; 2. results of an experiment to produce electron beams with instantaneous energy spread; 3. calculations of the coupling impedance of an electron ring to a squirrel cage structure.

1. Experiments in Pustarex

The main features of the Pustarex experiment are described in [1]; changes in the concept are given in [2,3]. In Pustarex the acceleration of ions - especially heavy ions - is to be accomplished in electron rings which are formed and accelerated in static fields, in between being compressed to higher density and larger internal field strength by pulsed fields. This concept was chosen to minimize the pulsed field energy to allow higher repetition rates and - with the static accelerating field - possible long accelerating structures. The accelerating length in Pustarex is about 1.3 m. Figure 1 illustrates the experimental setup.
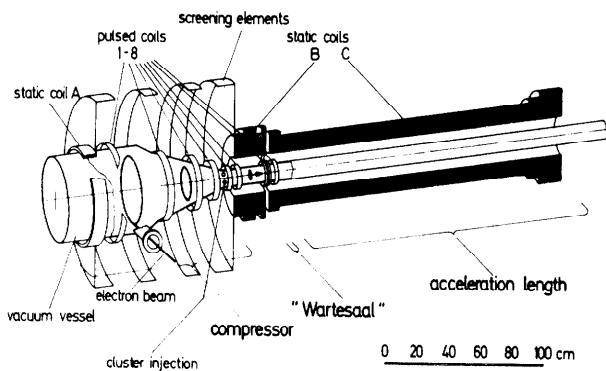
Three static coils A,B,C produce the magnetic mirrors for ring formation, the "Wartesaal", where trapped ions can be ionized to high charge states, and the diverging field for acceleration. The 8 pulsed coils compress the ring and transport it from the injection area to the Wartesaal and to the accelerator region. Acceleration of the electron rings is accomplished by the Lorentz force seen by the electrons rotating in the slightly diverging field. The radial field component B_r can be varied between 1 and 10 gauss with the help of additional static correction coils. Ions can probably be accelerated if the number of electrons in the ring is larger than 1×10^{12}.

The single-turn pulsed coils ensure rather fast compression of the electron ring. This has the advantage that the single-particle resonances are crossed rapidly and that at least for light ions no very low base pressure is required. On the other hand, the fast rising fields prevent the use of well conducting surfaces close to the ring, such as are needed to suppress the negative mass instability. Resistive wires, which were used originally [3], caused excitation of the resistive wall instability. With larger electron numbers (more than 3×10^{12}) this instability already led to almost total loss of electrons very early in the compression cycle.

This behaviour necessitated a tedious search for other ring environments with low coupling impedance. At first experiments were done with inner and outer squirrel cages. These had no positive effect. Squirrel cage structures have many resonances and average impedances far above that of a well conducting cylinder, as calculations described at the end of this report show.

If the rise time of the coil currents is not changed and resistive walls are excluded, capacitive walls with good azimuthal conductivity for the high frequencies (f > 250 MHz) of the negative mass instability and low conductivity for the frequency of the coils (f ~ 50 kHz) could be the solution of the problem. To get this, the eigenresonances of the capacitive wall had to lie between the coil frequency and the negative mass frequency. Figure 2 shows a schematic drawing of the capacitive walls finally used:

Fig.1: Schematic of the Pustarex Device
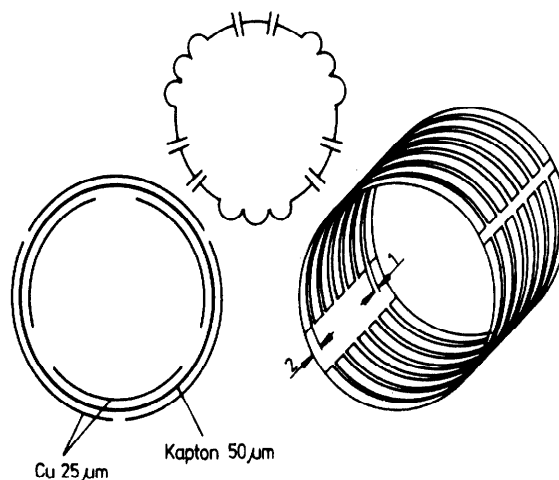
Fig.2: Schematic of the Capacitive Side Walls

*Max-Planck-Institut für Plasmaphysik, D-8046 Garching, Federal Republic of Germany

To avoid low-order particle resonances the rings have threefold symmetry. A 2 mm wide and 35 μm thick Cu ribbon on a 50 μm thick Kapton foil is slit at three azimuths 120° apart. To obtain an eigenresonance in the desired frequency range the slits are bridged on the inner side of the Kapton foil with a Cu ribbon of appropriate azimuthal width, thus forming a capacitive ring

with 6 capacitors. An equivalent circuit diagram is shown in Figure 2. The azimuthal width of the inner Cu foil is varied along the conical compression surface, so that the eigenfrequency is always an order of magnitude below the gyrofrequency of the electrons, the lowest harmonic of the negative mass instability.

This arrangement allows rapid field penetration and - as the axial width of the ribbons is only 2 mm - it does not appreciably influence the field components at the ring position. Although with larger particle numbers high-frequency activity is seen, which is probably due to the negative mass instability, particle losses, and hence also large ring widening, were not caused. A difficulty is still seen for the transition to the accelerating region. High ring velocities could excite the eigenfrequencies. Whether the rapid increase of the eigenfrequency in this region is sufficient to avoid this excitation has not yet been tested.

The structure described no longer acts - for distances of the order of the ribbon widths or larger - as a squirrel cage. This opens the possibility of using separate walls for focussing and impedance reduction.

As the Cu ribbons have good conductivity resistive instabilities are excluded. In the first experiments with very thin Cu ribbons this instability had led to drastic particle losses.

Although the resistive instability was excluded, the radial precessional mode became unstable during the sixth compression stage and roll-out phase and made compression and acceleration of rings with large particle numbers impossible. The nature of this instability is still unknown. As the degree of ionization from the background gas is almost 0.5% it could be the ion electron instability. Another possible origin could be misalignment of the squirrel cage to the field axis, which would produce a field disturbance for larger particle numbers only. Such a misalignment is not easily corrected, since the field axis is not known well enough and in the worst case might change in time and space for the combined pulsed and static fields. Our aim is therefore to improve the symmetry of the field producing currents. To reduce the growth rate of the ion electron instability, we shall install a better pumping system and increase the Landau damping in the critical regions. This could be done by a larger coil 6 and an external squirrel cage. Figure 3 gives the Landau damping coefficient for the present system with inner squirrel cage for low and high electron numbers and the same for the enlarged coil 6 with external squirrel cage.
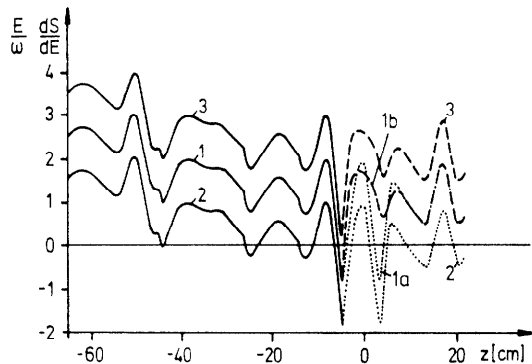
Fig.3: Landau damping coefficient. E = electron energy, $S = (1-\nu_r) \cdot \omega_0$, ν_r = single particle tune, ω_0 = electron revolution frequency, ω = radial collective frequency. Curve 1: no squirrel cage. 1a and 1b: old and new coils 6 resp. Curve 2: Inner squirrel cage with old coil 6, Curve 3: Outer squirrel cage with new coil 6.

It can be seen that in the present system the Landau damping coefficient can get very small for certain particle numbers.

In the Dubna experiment [4] this instability apparently was absent or at least did not cause particle losses. The reason may be increased Landau damping for heavily loaded electron rings. Accumulation of ions by impact ionization results in ion densities with a pronounced peak in the centre. If the ion loading is high enough, space charge results in strongly unharmonic transverse betatron oscillations of electrons which can enhance Landau damping of the transverse resistive wall instability. Based on a self-consistent equilibrium model [5] we have calculated the space charge potential of the electron and ion distributions with $f (= ZN_i/N_e)$ varying between 0.05 and 0.3, the last value corresponding to that of the Dubna experiment. The resulting radial tunes of electrons (ν_r) are plotted against the radial oscillation energy (Figure 4) for a case with R = 7.5 cm, n = 0.2, γ = 12 and N = 10^{13}. For f = 0.3 we find $\Delta\nu_r \gtrsim 0.5$, which stabilizes the dipole mode for arbitrary surface resistivities according to the approximate criterion $\Delta S \gtrsim 2|U+(1+i)V|$, $(S \equiv \omega_0(1-\nu_r))$. Whether this enhanced Landau damping can also stabilize the electron-ion instability at high levels of ion loading is still an open question.
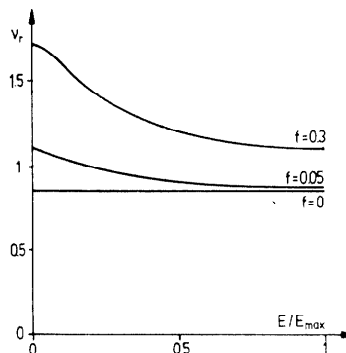
Fig.4: Dependence of radial tunes of electrons ν_r on transverse energy for different ion loading f

Electron rings with small particle numbers ($\sim$ 5 × 10^{11}) could be compressed and accelerated without instabilities and losses. The ring then maintained its integrity in the spill point, i.e. the electrons were not slowly wiped off, but the ring was transported as an entity into the accelerating region. Apparently the squirrel cage and/or ions gave enough focussing in the spill point. Figure 5 shows signals from a loop on axis and a Faraday cup that are placed about 25 cm beyond the spill point, 10 cm apart.
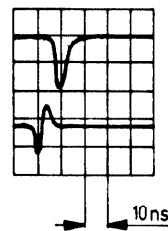
Fig.5: Signals of accelerated rings. Upper trace: Faraday cup. Lower trace: Signal of an axial loop, 10 cm before the Faraday cup.

The time difference of the signals gives a ring velocity of $\approx 1.7 \cdot 10^9$ cm/s and the width of the Faraday cup signal suggests axial dimensions of about 3 cm. The ring velocity can be reduced by smaller radial fields. A thorough investigation of ion acceleration has been postponed until rings with larger particle numbers can be accelerated.

2. Development and Investigation of Finite Energy Spread and Improved Emittance Electron Beams

Some of the collective instabilities that impose upper bounds on the holding power of the electron rings can be suppressed by Landau damping of the electrons having an instantaneous finite energy spread. In previous electron ring experiments the energy spreads were produced by passing the beam through non-uniform energy absorbers [6,7,8] that, besides spreading the electron energy, also increase the electron beam emittance undesirably.

As proposed by the Karlsruhe ERA group [9], a controllable energy spread of the electrons can be produced by using separate cathode elements resistively coupled to the high-voltage terminal. In contrast to this proposal the cathode elements in our experimental device are not arranged coaxially but in a row. This allows the electrons to be injected after passage through the beam transport system approximately on their closed orbits, thus minimizing their radial betatron oscillations.
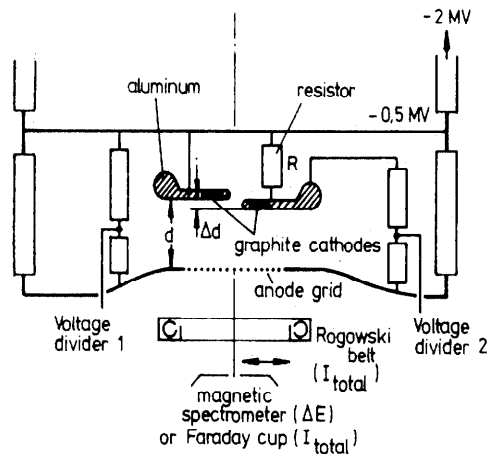
Fig.6: Schematic of the Experimental Device

The experiments are performed using an electron beam generator (Febetron 705) and a modified beam tube (see Figure 6). The cathode is split radially in two halves (division into several parts is intended), which can be separately placed at different distances from the grid electrode and connected via different resistors R to the high-voltage terminal. This arrangement allows measurement of the potential difference of the two cathode halves and hence deduction of the electron energy difference ΔE and - with the resistance R - the current I_2. The total current I_{total} is measured with a Rogowski coil downstream from the anode grid, and independently by the Faraday cup measurement. The magnetic spectrometer allows verification of the electron distribution as obtained from the voltage divider measurements.

The formerly applied cathode elements made of pins or razor blades are replaced by plane solid graphite cathode elements [10] since these elements - as the measurements indicate already - give small beam emittances. Great effort has been expended on the choice of the structure and material of the plates surrounding the cathode elements and determining the potential distribution in the diode in order to reduce and suppress parasitic electron emission from these surfaces. Aluminum proved to be an appropriate material for suppression of parasitic emission at a cathode-to-anode grid distance of d = 1.5 cm.
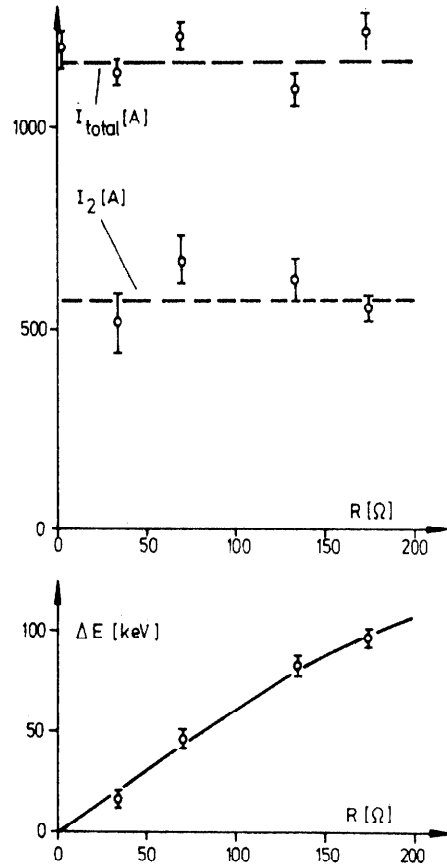
Fig.7: Total current I_{total}, current I_2 from the cathode half containing the resistor, and electron energy difference ΔE versus R
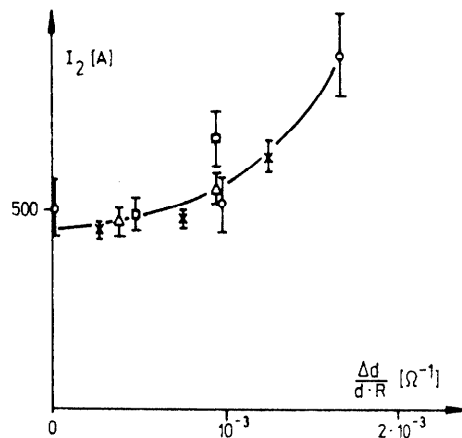
Fig.8: Partial current I_2 versus normalized cathode spacing

Some experimental results are shown in Figures 7 and 8. In Figure 7 the total electron current I_{total} and the partial current I_2 (from the cathode half with the resistor) as well as the electron energy difference ΔE (at the time of maximum current) are plotted versus the resistance R. It is found that I_{total} and I_2 (with Δd chosen such that both cathode halves have approximately equal field strengths) are nearly independent of R, and that both cathode halves emit about equal currents, i.e. I_2 is about half the value of I_{total}. Moreover, the energy difference ΔE increases about linearly with R (at a slope of 0.6 keV/Ω and reaches a value of ΔE = 100 keV with about 170 Ω, which corresponds to the desired relative energy difference of $\Delta E/E \approx 5\%$ at 2 MeV electron energy.

In Figure 8 the partial current I_2 is plotted versus the distance Δd of both cathode elements (see Figure 6) normalized to d and to the resistance R. The data points - the same resistances R are indicated by the same symbols - can be roughly represented by one curve. The current I_2 reaches about half the total current for $\Delta d/(R \cdot d) \approx 10^{-3} \, \Omega^{-1}$, which corresponds to cathode spacings such that the mean electric field strength in both diode halves is about equal. As demonstrated by particle trajectory calculations, the beam emittance is minimum in this case.

The next series of experiments will be carried out with the cathode device at a potential of -2 MV (and the grid at -1.5 MV) to study the beam transport to the injection snout and measure the spatial and energetic distributions as well as the beam emittance in the injection plane.

3. Longitudinal Coupling Impedance of an Electron Ring in a Squirrel Cage

Axially slit conducting cylinders, so-called "squirrel cages", have been successfully used for axial focussing of the ring. Since its longitudinal stability also strongly depends on the geometry of nearby conducting walls, it is necessary to investigate quantitatively the influence of a squirrel cage on the negative mass instability by calculating the coupling impedance matrix $Z_{m,n}$ of the ring inside or outside a squirrel cage. The impedance of an E-layer inside a squirrel cage has been calculated by Beloshitsky and Perelshtein [11]. In the present paper we consider the impedance of an electron ring infinitely thin in the radial direction and with an axial length 2a. The electrons rotate coaxially inside or outside a squirrel cage of radius T consisting of N strips of width D and slits of width L-D (Fig.9).
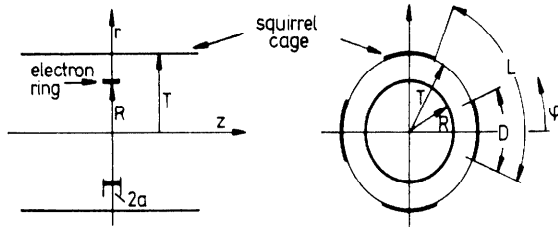
Fig.9: Schematic of Squirrel Cage Configuration

The impedance matrix $Z_{m,n}$ is defined by

$$\overline{E}_{\varphi,m} = -\frac{1}{2\pi R} \sum_{n=-\infty}^{+\infty} Z_{m,n} I_n , \tag{1}$$

where $\overline{E}_{\varphi,m}$ is the m-th Fourier component of the electric field at ring radius R averaged over the ring length 2a. The electric field is produced by a charge and current density perturbation ρ, j_φ. The current is given by

$$j_\varphi = \sum_{n=-\infty}^{+\infty} I_n \delta(r-R) \left(\frac{\Theta(z+a) - \Theta(z-a)}{2a} \right) e^{i(n\varphi - \omega t)} , \tag{2}$$

where $\Theta(z)$ is the Heaviside function. The charge density follows from the continuity equation $\dot{\rho} + \text{div} \, \underline{j} = 0$.

Maxwell's equations satisfying the periodic boundary conditions on the conducting strips $E_{\text{tangential}} = 0$ were solved using a method by which the problem is reduced to a Hilbert problem [12,13]. The only non-vanishing elements of the impedance matrix $Z_{m,n}$ obtained are those for which $m = N\ell+n$, $|\ell| = 0, 1, 2, \ldots$ One gets

$$Z_{N\ell+n,n} = \delta_{N\ell+n,n} Z_n^{ri} + Z_{N\ell+n,n}^{sq} , \tag{3}$$

with

$$Z_n^{ri} = 4\pi^2 \int_0^\infty \left(\frac{n^2 k^2}{s^2 \omega} b_n(R,R) + \omega R^2 b_n'(R,R) \right) \frac{\sin^2 ka}{k^2 a^2} \, dk , \tag{4}$$

and

$$Z_{N\ell+n,n}^{qu} = -4\pi^2 \int_0^\infty \left(\frac{i\pi N(N\ell+n)n k^2}{\omega s^2} b_n(R,T) b_{N\ell+n}(R,T) x_{\ell+m_0} \right. \tag{5}$$

$$\left. - \frac{i\pi s^2 R^2 T^2 \omega}{N} b_n'(R,T) b_{N\ell+n}'(R,T) y_{\ell+m_0} \right) \frac{\sin^2 ka}{k^2 a^2} \, dk ,$$

where $s = \sqrt{\omega^2 - k^2}$, and $m_0 \geq 0$ is an integer such that $m_0 = \frac{n}{N} - \mu$, $0 \leq \mu < 1$. Z_n^{ri} is the ring impedance in free space and $Z_{N\ell+n,n}^{sq}$ is the contribution due to the squirrel cage. The path of integration in equ.(5) has to be taken below the pole at $k = \omega$. The b_n, b_n' are products of Bessel and Hankel functions J_n, $H_N^{(1)}$ and their derivatives J_n', $H_n^{(1)}$:

$$b_n(r,T) = \begin{cases} J_n(sr) H_n^{(1)}(sT), & r \leq T \\ \\ J_n(sT) H_n^{(1)}(sr), & r > T \end{cases} \tag{6}$$

and

$$b_n'(r,T) = \begin{cases} J_n'(sr) H_n^{(1)'}(sT), & r \leq T \\ \\ J_n'(sT) H_n^{(1)'}(sr), & r > T \end{cases} \tag{7}$$

The coefficients x_m, y_m are the solutions of an infinite system of linear equations:

$$\sum_{m=-\infty}^{+\infty} \left(\frac{\delta_n^m}{m+\mu} - \frac{\eta_m}{|m+\mu|} W_n^m \right) x_m = W_n^{m_0} , \tag{8}$$

$$\sum_{m=-\infty}^{+\infty} (\delta_n^m - |m+\mu| \epsilon_m T_n^m) y_m = T_n^{m_0} ,$$

where δ_n^m is the Kronecker symbol and the η_m, ϵ_m are given by

$$\eta_m = 1 - i\pi N |m+\mu| b_{N(m+\mu)}(T,T) , \tag{9}$$

$$\epsilon_m = 1 + \frac{i\pi s^2 T^2}{N |m+\mu|} b_{N(m+\mu)}'(T,T) ,$$

The matrices W_n^m and T_n^m are defined by

$$W_n^m = m U_n^m + \frac{\mu}{n+\mu} \frac{1}{2} \left(P_{n-1}(u) + \frac{P_\mu(-u)}{P_{\mu-1}(-u)} P_n(u) \right) P_m(u) , \tag{10}$$

$$T_n^m = \frac{m}{m+\mu} U_n^m + \frac{\mu P_m(u)}{(m+\mu)(n+\mu)} \frac{1}{2} \left(P_{n-1}(u) - \frac{P_\mu(u)}{P_{\mu-1}(u)} P_n(u) \right) ,$$

with

4175

$$U^m_n = \begin{cases} \dfrac{1}{n-m} \cdot \dfrac{1}{2}\left(P_m(u)P_{n-1}(u) - P_{m-1}(u)P_n(u)\right), & n \neq m \\[12pt] \dfrac{1}{|n|} \cdot \dfrac{1}{2}\sum_{\ell=0}^{|n|-1} \dfrac{P_\ell(u)\cdot(P_{\ell-1}(u)-P_{\ell+1}(u))}{2\ell+1}, & n = m,\ n \geq 1 \\[12pt] -\ln\dfrac{1+u}{2} & n = 0,\ m = 0 \end{cases} \qquad (11)$$

The $P_m(u)$, $P_\mu(u)$ are Legendre functions of the argument $u = \cos(\pi D/L)$.
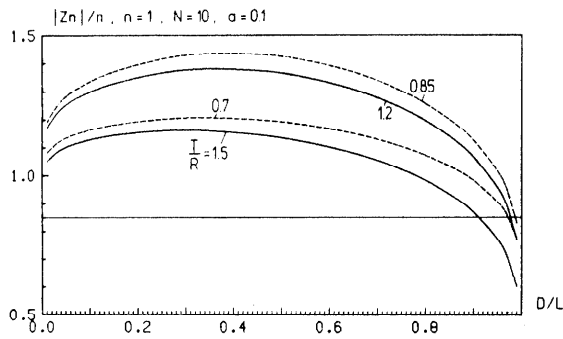
Fig.10: The first harmonic of $|Z_n|/n$ in units of Z_o
[$= 377\ \Omega$] is plotted as a function of the strip width for different squirrel cage radii T.

The equation for x_m and y_m converge rather quickly so that one needs only few equations to obtain sufficiently correct results. In Figure 10 the absolute value $|Z_{n,n}|/n$ for $n = 1$ is shown as a function of the strip width D for different T. One can restrict the discussion to the diagonal elements $Z_{n,n}$, because in most cases consideration of the off-diagonal elements gives a small correction only in the linear stability analysis [14]. The surprising result is that $|Z_{n,n}|$ exceeds the ring in free space values and very slowly approaches the lower impedance of the ring in a conducting cylinder as the slit width goes to zero. The reason for that is that the pole contribution of $k = \omega$ in the integral (5) leads to a considerable increase of the real part of $Z_{m,n}$. In terms of the electromagnetic mode expansion this is a TEM mode, a wave proportional to $e^{-i\omega(|z|-t)}$ and propagating undamped along the squirrel cage surface [15].
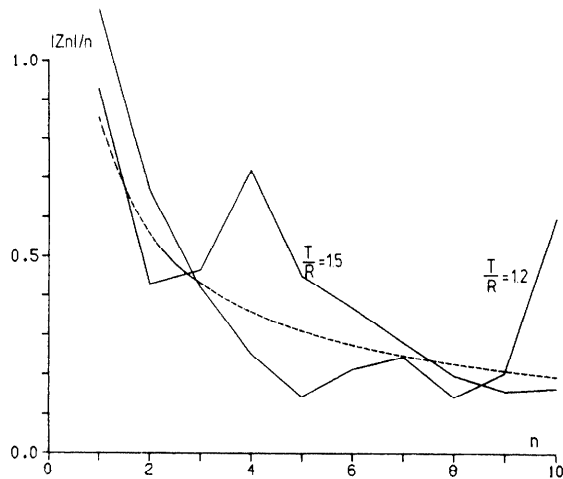
Fig.11: $|Z_{n,n}|/n$ is plotted as function of n for different squirrel cage radii T, number of strips N=10, and a strip to slit ratio of D/(L-D)=0.85. Dashed curve: impedance of the ring in free space.

In Figure 11 the impedance $|Z_{n,n}|/n$ is plotted as function of n for different T and a strip to slit ratio of D/(L-D) = 0.85. The number of strips is N = 10. In a squirrel cage of finite length this effect will be substantially suppressed. To give an example of the rather complicated dependence of $Z_{n,n}$ on the different parameters n, N, u and T, the real and imaginary parts of $Z_{n,n}/n$ are plotted as functions of T for n = N = 10 (Figure 12).
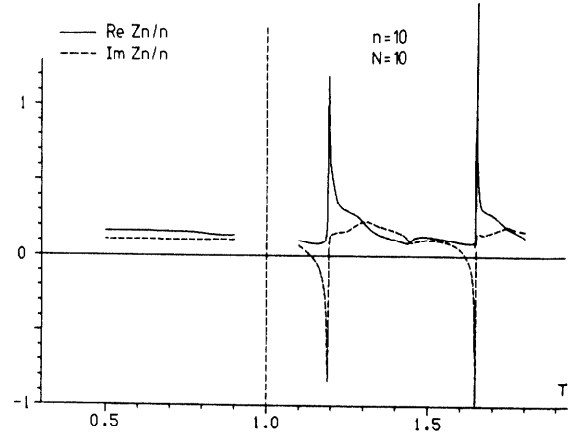
Fig.12: The real and imaginary parts of $Z_{n,n}/n$ (n = 10) in units of Z_o (= 377 Ω) for a strip to slit ratio of D/(L-D) = 0.85 as function of T/R. Number of strips N = 10

References

1 W. Herrmann, Proc.of the II Symp.on Coll.Methods of Acceleration, Dubna 1976
2 C. Andelfinger et al., Proc.of the 1977 Part.Accel. Conf., Chicago/USA, p.1622-1624 (1977)
3 C. Andelfinger et al., Proc.of the IV All-Union Conf., Dubna 1978
4 G.V. Dolbilov et al., Dubna Report, JINR P9-11191, Dubna 1978
5 I. Hofmann, Proc.9th Int.Conf.on High Energy Accel. Stanford/USA (1974), p.245
6 A. Faltens et al., Proc.9th Int.Conf.on High Energy Accel., SLAC, Stanford/USA, 1974, p.226
7 J. Fink, W. Ott, MPI f.Plasmaphysik, Garching, Report IPP 0/17 (July 1973)
8 U. Schumacher, M. Ulrich, Proc.II Symp.on Coll.Meth. of Acceleration, Dubna 1976, p.38
9 C.H. Dustmann et al., Proc.9th Int.Conf.on High En. Accelerators, SLAC, Stanford/USA, 1974, p.250
10 R.K. Parker et al., J.Appl.Physics 45, 2463 (1974)
11 P.F. Beloshitsky, E.A. Perelshtein, JINR-P9-11195 Dubna (1978)
12 Z.S. Agranovich et al., Sov.Phys.Tech.Phys.7, 277, (1962)
13 S.S. Tretyakova et al., Sov.Phys.Tech.Phys.12, 1413 (1968)
14 E.S. Masunov, Sov.Phys.Tech.Phys.19, 1185 (1975)
15 P. Merkel, Proc.3rd Int.Conf.on Coll.Meth.of Accel. Irvine 1978